Geochemical modeling of solid waste-binder systems in stabilization/solidification applications

Yikai Liu

Dipartimento di Geoscienze e Centro CIRCe, Università degli Studi di Padova, via G. Gradenigo 6, 35129, Padova, Italia
DOI:10.19276/plinius.2023.01.007

INTRODUCTION

Sustainable soil stewardship provides the basis for terrestrial ecosystems and geochemical cycles. However, the unprecedented urbanization in the last decades brought massive solid waste stockpiles worldwide, detrimental to soil health and the neighborhood flora and fauna.

Herein, in-situ solidification/stabilization (S/S) has been proposed as a remediation strategy to prevent further pollution in the contaminated sites. But the challenges of substantial CO_2 emission and the sensitive durability attributed to ordinary Portland cement (OPC), which is the most widely used binder in the S/S technique, place this strategy under scrutiny. Herein, developing alternative low-carbon and cost-effective binders is important for facilitating these traditional remediation technologies.

In this work, we examined the feasibility of mitigating or negating the use of OPC in the S/S process of pyrite ash and phosphogypsum, the primary hazardous solid wastes generated in the phosphate industry. One traditional binder (OPC) and four alternative low-carbon footprint binders (calcium aluminate cement (CAC), white-steel-slag activated blast furnace slag (GGBFS), alkaline-GGBFS, and OPC-GGBFS) were applied in the remediation process. After the physicochemical and mineralogical characterization of the stabilized products, we constructed the geochemical modeling to reveal the potential mechanisms of contaminant retention and ensure long-term environmental availability. Finally, we evaluated how integrating these innovative technologies could shed light on reducing greenhouse gas emissions and offer technical benefits in future field trials.

The overall findings underscore the immobilization mechanisms of pollutants using different binder strategies and highlight the urgent need to bridge the zero-emission insights to sustainable S/S technologies. The constructed geochemical modeling, in tandem with the inclusion of more solid waste types and properties in the following models, will be pivotal in predicting the availability and efficiency of green and sustainable remediation strategies.

WASTE CHARACTERIZATION

The waste used in this work was excavated from an abandoned fertilizer production facility in Italy, which is now used as a storage site for the solid waste generated by pyrite roasting, sulfuric acid production, and phosphorus fertilizer production. The contaminated soil was collected following a systematic sampling grid from the surface to 2.5 m depth covering the whole area of around 0.11 km². In this work, the soil was mainly composed of black pyrite ashes. The soil sample was placed in a polyethylene bag and then transported to the laboratory. Then the sample was air-dried, ground, and passed through a 2 mm mesh sieve prior to the following characterization experiments.

Characterization of pyrite ash

The SEM images (Fig. 1a, b, and c), as well as the XRD investigations, evidence the presence of hematite, jarosite, gypsum, quartz, and anglesite (Liu et al., 2023b). Besides forming sparingly soluble anglesite at acidic conditions, Pb was found in complex exsolution/intergrowths textures in amorphous Fe oxide phases (Fig. 1d and e) and incorporated in the Fe-K-S-Pb oxide rims in a compact form along the edges of the structures (Fig. 1f and g). The presence of Fe-K-S-Pb oxide rims could imply Pb incorporation within the jarosite crystal structure. In addition, the fate of Zn was related to the formation of sulfur minerals, as a Zn-Fe-S assemblage was observed in Fig. 1i. But as a minor component, it is hard to assess the exact origins of this assemblage, which may represent a residue of the primary ore or a precipitated secondary phase.

To analyze the Pb distribution mechanisms in the contaminated soil, Raman spectroscopy was further used to examine the area with high Pb concentration presented in Fig. 1d and g. The results imply the presence of kintoreite and Pb incorporation into jarosite.
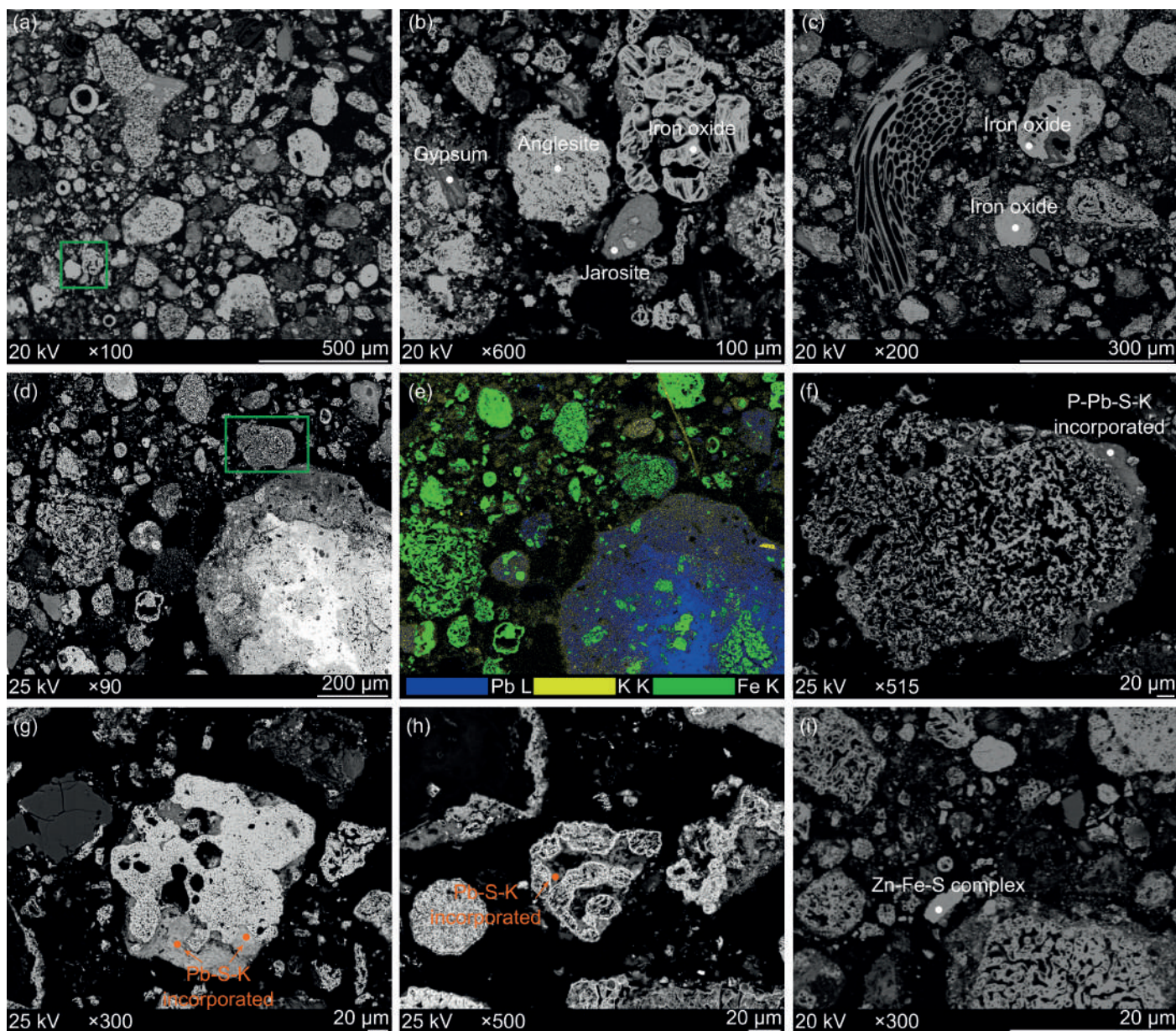
Figure 1 SEM micrographs of the sample. a) backscattered scanning electron (BSE) microscopy image of contaminated soil. b) BSE image showing the presence of anglesite. c) BSE image implies the iron oxide; d) BSE image demonstrates the distribution of Pb. e) elemental mapping of lead, potassium, and iron attributing to image d. f) the magnified BSE image corrected to the green rectangle marked area in image d, indicating a Pb-incorporated structure. g) and h) the compacted Pb-bearing assemblages. and i) BSE image shows the Zn-Fe-sulfate assemblage.

Leachability of potentially toxic elements

When using deionized water as the leachate (at pH 4.6), the leachability of the tested elements showed that the contaminated soil should be classified as hazardous waste, with all the concentrations being significantly higher than the limits established by Italian laws. The leaching of the studied trace metals (Pb, Zn, and Fe) showed a strong dependence on the pH values, indicating that the contaminated soil is susceptible to changing conditions of the stockpile.

At the pH value of 1.98, the highest concentrations of Pb, Zn, and Fe in the leachate were reached at 1.59×10^1, 7.49×10^1, and 2.69×10^2 µmol/L. The minimum release of Pb (0.38 µmol/L) and Zn (0.30×10^{-1} µmol/L) was found at the pH value of 9.04. However, with the increase in pH values, Pb and Zn showed an upward tendency in the release under alkaline conditions. The enhanced element release at basic conditions was due to the occur-rence of specific dissolution of minerals (e.g., the transformation of Pb/Zn bearing carbonates to hydroxides) and desorption reactions of elements from reactive surfaces (e.g., Pb/Zn may desorb from Fe-oxides surfaces and favor the formation of hydroxyl-complexes). By contrast, the release of Fe at the neutral/alkaline conditions fluctuated approximately from 0.32 to 3.40 µmol/L, which was probably related to the formation of iron hydroxide. Besides, the increasing leachability of SO_4^{2-} was only observed under alkaline conditions, with the concentrations being constant at around 104 µmol/L in the acidic and neutral regions.

HIGH-PERFORMANCE S/S (HPSS) TO WASTE

Solidification/stabilization (S/S) is a mature industrial process for the remediation of solid waste containing hazardous substances (Calgaro et al., 2021; Contessi et al.,

Figure 2 HPSS® process framework.

2020). Typically, as one of the most widely used artificial materials in industries (Habert et al., 2020; Bui Viet et al., 2020), ordinary Portland cement (OPC) is extensively applied in the S/S process due to its unique properties and simplicity of use (Hou et al., 2023; Ouhadi et al., 2021). However, the substantial carbon dioxide emission during OPC production and the concerns about its undesirable retention capacity for potentially toxic elements strain this strategy.

To tackle this objective, we herein tailored four alternative binders (CAC, OPC-activated GGBFS, white-steel-slag activated GGBFS, and alkaline-activated GGBFS) for facilitating immobilization of high Pb content pyrite ash, with the perspectives of enhancing Pb retention and mitigating anthropogenic carbon dioxide emissions.

Given in Fig. 2 is the framework of the high-performance S/S (HPSS®) process proposed by our co-workers (Bonomo et al., 2009; Contessi et al., 2020). After removing the large aggregates of the collected contaminants, the sieved sample and binder, primarily cementitious materials, are blended in a mechanical disc pelletizer with a predetermined amount of aqueous solution (water or alkaline solution). Then the pellets are cured in air or atmosphere-isolated conditions for subsequent real-world use.

This management is deemed to effectively convert the solid waste to a physiochemically stable solid assemblage that can long-term or permanently store contaminants in a relatively less mobile form (Chen et al., 2009).

HPSS of natural resource-derived binders

In OPC-based pellets (OP), typical crystalline hydration products of OPC (ettringite, 5.5 wt%) and unhydrated clinker phases (Alite and Belite, 1.6 wt% in total) were clearly detected in its XRD pattern (Fig. 3a). Hematite (54.0 wt%), jarosite (2.1 wt%), and gypsum (6.7 wt%), originating from the raw pyrite ash, were also present. The amorphous content, primarily composed of C-S-H gel, was quantified as 24.2 wt%. The absence of portlandite is possibly related to the carbonation with the atmospheric CO_2 because approximately 4.4 wt% of calcite was observed (Du et al., 2019).

XRD mineralogical analyses of the CAC-based samples (CA) show that the amount of precipitated ettringite (15.1 wt%) is approximately triple of the CP samples. This is because the CAC binder is mainly composed of $CaO \cdot Al_2O_3$ (CA), $CaO \cdot 2Al_2O_3$ (CA2), and $12CaO \cdot 7Al_2O_3$ (C12A7), thus producing considerable aluminum-containing hydration products, as ettringite and gibbsite (4.3 wt%) present in CA samples. In turn, the amorphous content (10.7 wt%) is only half of the CP samples, possibly assigned to amorphous aluminum hydrates, instead of the C-S-H gel precipitation as in the CP system (Hidalgo et al., 2009; Li et al., 2017).

SEM/EDS analysis of OP samples shows that the dark rims around the unhydrated OPC particles are C-S-H gel, which is the typical amorphous hydration product of the OPC system, as high Ca and Si weight fractions detected. The presence of Pb is observed in the mixtures of pyrite ash phases and cementitious matrices adjacent to the iron oxide particles and is preserved in the C-S-H. In CA samples, more cracks are observed throughout the analyzed areas, which could be attributed to ettringite dehydration due to the oven drying process during the sample preparation (Bizzozero et al., 2014) and the high vacuum condition reached in the SEM experiments (Contessi et al., 2020). SEM/EDS analysis of OP samples shows that the dark rims around the unhydrated OPC particles are C-S-H gel, which is the typical amorphous hydration product of the OPC system, as high Ca and Si weight fractions detected. The presence of Pb is observed in the mixtures of pyrite ash phases and cementitious matrices adjacent to the iron oxide particles and is preserved in the C-S-H.

In CA samples, more cracks are observed throughout the analyzed areas, which could be attributed to ettringite dehydration due to the oven drying process during the sample preparation (Bizzozero et al., 2014) and the high vacuum condition reached in the SEM experiments (Contessi et al., 2020). The presence of Pb in CA pellets has a high correlation with the spatial distribution of Ca, Al, Fe, and S, inferring that Pb-bearing species are well-intermixed with ettringite through the adsorption
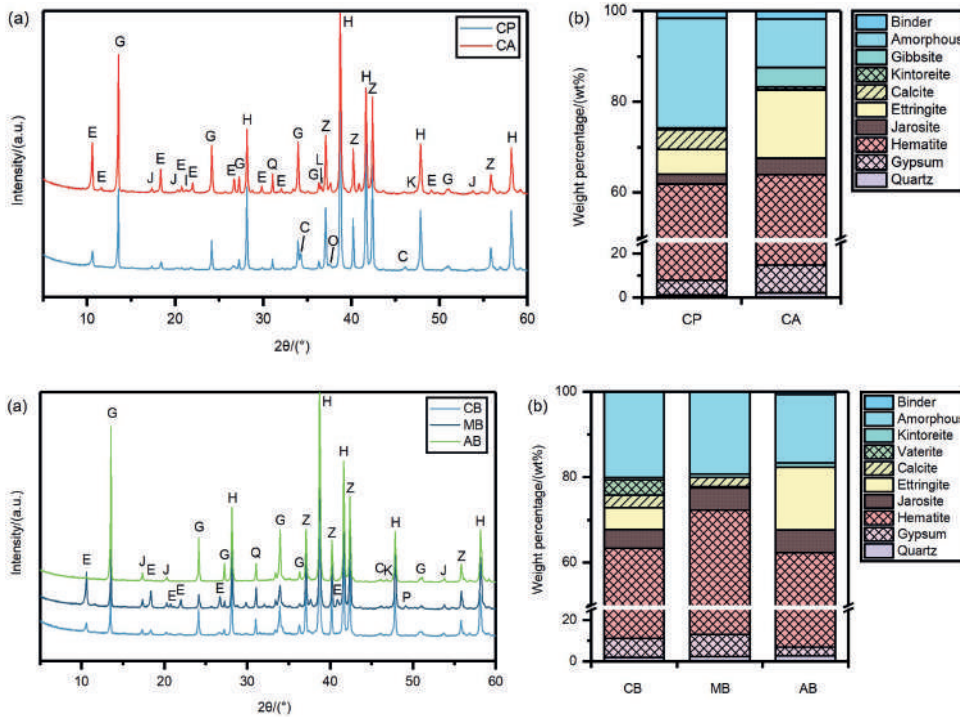
Figure 3 XRD characterization of CP and CA samples. (a) The detected XRD spectra and (b) The correlated quantification results. C: calcite, E: ettringite, G: gypsum, H: hematite, I: Gibbsite, J: jarosite, K: kintoreite, L: gehlenite, O: alite and/or belite, Q: quartz, and Z: zincite. Binder in Fig. 3b indicates the sum fraction of alite and belite in CP samples and the gehlenite fraction in CA samples.
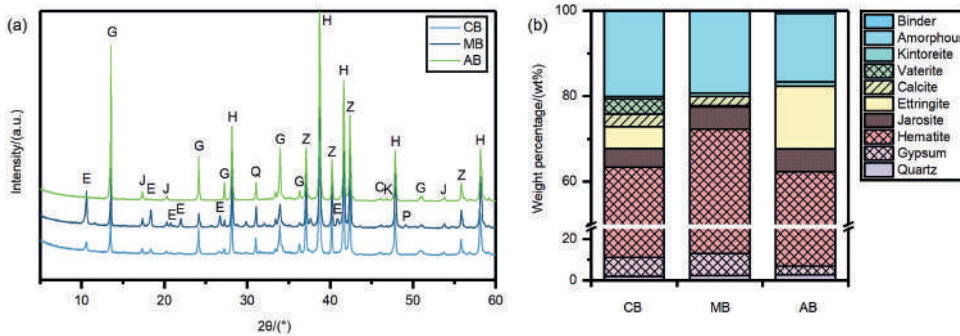

Figure 4 XRD characterization of CB, MB, and AB samples. (a) The detected XRD spectra and (b) The correlated quantification results. C: calcite, E: ettringite, G: gypsum, H: hematite, J: jarosite, K: kintoreite, Q: quartz, and Z: zincite. Binder in Fig. 4b indicates the sum fraction of alite, belite, and gehlenite fraction.

and/or incorporation.

HPSS of by-products-derived binders

The XRD results of CB pellets (Fig. 4a and b) illustrate that hematite is the main crystalline phase detected (52.0 wt%). Meanwhile, jarosite and gypsum, also originating from the pyrite ash, are observed at 4.4 and 9.2 wt%, respectively. The binder hydration products are ettringite (5.1 wt%) and amorphous phases (20.1 wt%) that mainly consist of C-(A)-S-H gel and unreacted slags (Berthomier et al., 2021). Carbonates (vaterite and calcite) deriving from the carbonation of calcium species (e.g., portlandite and gypsum) at alkaline conditions are quantified as 6.6 wt%. A minor proportion (0.5 wt%) of the crystalline Pb-bearing phase kintoreite is found, with the most pronounced diffraction peak being observed at 46.8° 2θ.

MB samples present similar hydration products as the CB scenario, however, with more crystalline ettringite (14.7 wt%) and fewer amorphous contents (16 wt%). Accordingly, the sulfate contents (gypsum 4.2 wt% and jarosite 5.3 wt%) are decreased. The carbonate species detected in CP and CB pellets are not present in the MB samples, indicating the low concentration of calcium in the pore solutions, which is not conducive to the formation of portlandite and its subsequent carbonation. Further, although high aluminum content steel slag and GGBFS are aluminate-rich materials like the CAC binder, the crystalline gibbsite is not observed in the XRD spectra of MB samples.

XRD mineralogical analyses of the AB pellets show that the ettringite formation is inhibited in this system (0.3 wt%). Likewise, the phases originate from pyrite ash (hematite (59.0 wt%), gypsum (10.9 wt%), jarosite (5.2 wt%), quartz (2.3 wt%), and kintoreite (0.9 wt%)) account for

over 75 wt% of the quantified pellets fraction, implying a relatively low hydration degree in AB samples. Note, the amorphous fraction in CB, MB, and AB samples can also be partially attributed to unhydrated GGBFS, which are amorphous (Gardner et al., 2015; Kirca et al., 2013).

Leachability of Pb and carbon emissions estimation of each binder scenario

The results of ultrapure water leaching (Fig. 5) confirmed the immobilization efficiency of Pb in the collected pyrite ash and applied binder scenarios, as well as the detected leachability of Al, Fe, and sulfates. Without the HPSS process, the release of Pb (1900 μg/L) from the pyrite ash is two orders of magnitude higher than the limits (10 μg/L based on D.Lgs. n. 152/2006 and 50 μg/L based on D.M. n. 186). In the CP pellets, the Pb leachability (180 μg/L) far exceeded the concentration limit for on-site reuse (10 μg/L), which confirms previous results showing that the OPC binder is insufficient when the Pb concentration is in a relatively high range (Contessi et al., 2020). The Pb leachability of CB, CA, and MB decreased to 30, 20, and 57 μg/L, respectively.

In addition, Fig. 5 summarizes the carbon emissions and the preparation cost associated with each binder scenario. CP pellets show the largest carbon footprint, as recycling 1 tonne of pyrite ash will release 215 kg of CO_2. Considering the CO_2 saving in view of the samples in its use stage by reacting with atmospheric CO_2 (Habert et al., 2020), CP carbonation can eliminate 29.7 kg CO_2/t of the carbon footprint, which is approximately 14% of the precursor pelletizing process. Herein the overall cost for the CP pellets preparation could reach 30.8 €/t (17.8 from the binder and water supply and 13.0 from the estimated CO_2 tax in E.U.). With regard to CA pellets, the overall cost related to the pelletization process could
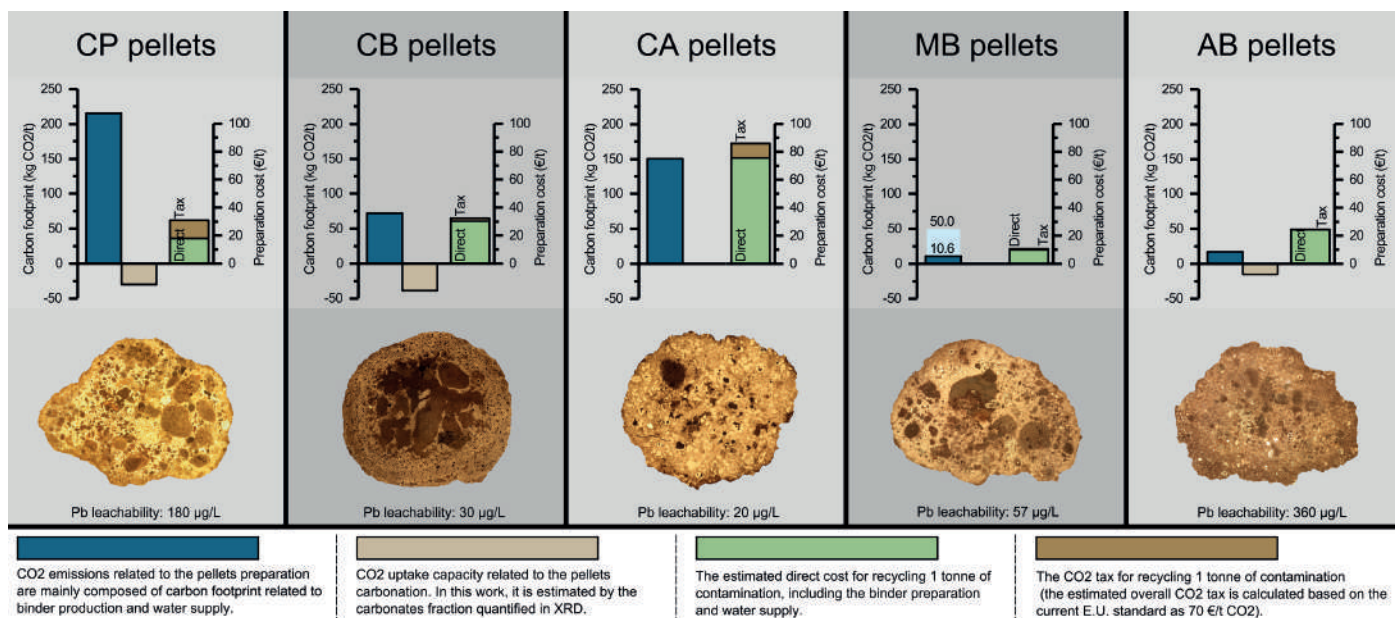
Figure 5 *The optical microscope images and the related carbon footprint of the pellets preparation. The carbon uptake of CA and MB pellets is estimated to be 0 because the carbonates are not found in their XRD patterns. The "Direct" represents the direct cost related to the pellets preparation and the "Tax" indicates the indirect cost of CO_2 tax. Note that the carbon footprint and CO_2 tax of MB pellets are estimated based on recycled steel slag (10.6 CO2/t CO_2 emission, 10.0 €/t direct cost, and 0.7 €/t CO_2 tax), while the bright blue column marked indicates the estimation is from synthetic mayenite, which is the primary component of recycled steel slag (50.0 CO2/t CO_2 emission, 12.8 €/t direct cost, and 3.5 €/t CO_2 tax).*

make this strategy unprofitable (75.5 €/t) because of the high price of CAC binder and its production is less carbon-negative, which may emit 150.5 kg CO_2/t. Further, the inhibited carbonation in CA pellets may bring less CO_2 tax benefit to this strategy.

With the substitution of industrial by-products, the CO_2 benefits under CB, MB, and AB options are optimized accordingly. The calculated CO_2 release and uptake of CB samples are 71.9 and 38.7 kg CO_2/t, indicating that more than half of the CO_2 emission related to binder production can be mitigated as a consequence of the sponge effect. Although the CB binder preparation cost (30.2 €/t) is higher than the CP pellets, the CO_2 tax (2.3 €/t) is much less than the traditional pathway. For the MB pellet, despite the carbonates (calcite and vaterite) are also not found in this sample, its associated carbon footprint is only a quarter of the CP preparation at 50.0 kg CO_2/t. Meanwhile, because of the broad quantities and economics of GGBFS, the overall cost of the MB scenario is only 10.0 €/t. The lowest carbon footprint corresponds to the cases of AB pellets, with the emission estimated as 16.9 kg CO_2/t. The following carbonation takes up 15 kg of CO_2 emissions.

GEOCHEMICAL MODELING SUMMARY

Characterizing the PTEs leaching behaviors and the associated mechanisms over a broad pH range is fundamental in tailoring the field application. However, relevant empirical analysis to reveal the underlying mechanisms responsible for the leaching behavior of constituents remains poorly understood.

Based on recent studies, the geochemical modeling approach could disentangle how this coupling operates, where insights can be gained through the use of pH-dependent leaching tests in association with geochemical speciation modeling (Chen et al., 2021; Du et al., 2019; Jarošíková et al., 2018; Sun et al., 2019). The dissolution/ precipitation equilibrium of the PTEs-containing phases and the cementitious assemblages is assumed to be the primary mechanism for the leaching behavior of the PTEs. However, there is strong evidence that the ion exchange and adsorption also play a critical role in controlling the PTEs release, for instance, the Pb could be incorporated into the ettringite structure (Contessi et al., 2021) and adsorbed onto the surface of C-S-H/C-A-S-H gel (Chen et al., 2022; Liu et al., 2021). The reconstruction of these processes in geochemical modeling is still fragmented and poorly constrained (Vega-Garcia et al., 2021; Zavarin et al., 2022). This is because the representativeness of the modeling is limited by the amount of available data from the thermodynamic database (Holmes et al., 2022; Lu et al., 2022). These knowledge gaps hinder the development of a fundamental understanding of the controls on PTEs release and migration.

To contribute to filling in these gaps, we elucidated the roles of traditional (OPC) and alternative (CAC) binders in Pb retention, thus addressing the relatively low Pb immobilization efficiency associated with conventional OPC and (2) integrating the insights into the adsorption and ion exchange mechanisms controlling Pb mobilization. With the thorough characterization of the partitioning of chemical species, we constructed geochemical modeling coupled with the Parameter Estimation software (PEST). By comparing the identified PTEs' leaching behavior from experiment and simulation, we investigated and quantitatively classified the impacts from dissolution/precipitation, adsorption, and physical encapsula-

tion on Pb capture. The results of this paper demonstrate the feasibility of using the Portland-free pathway to immobilize the PA. Further, it provides a reliable methodology to guide and test the plausibility of conceptual and numerical models of Pb mobilization and transport, even with a limited dataset, which may contribute to a more complete picture of PTEs release mechanisms in the stabilized products and improve the trail application of S/S technologies.

Quantification of Pb and sulfates retention in OPC- and CAC-based pellets.

Fig. 6 gives the quantitative results of the Pb and sulfates-bearing species of OP and CA modelings under the studied pH ranges. At alkaline pH conditions (pH > 8), the immobilization of Pb in the OP samples mainly relies on the adsorption and ion exchange capabilities of C-S-H and ettringite. With the decrease in pH values, the neutral pH conditions are no more suitable for the equilibrium of C-S-H and ettringite (Liu et al., 2023a).

Therefore, the adsorbed Pb is gradually released as a consequence of the dissolution of hydration products. Then the soluble Pb precipitates as cerussite or is partially immobilized by the ferrihydrite ($Fe(OH)_3$) and hematite. At acidic conditions (pH < 5), the Pb immobilization is attributed to the anglesite precipitation and hematite adsorption. However, non-negligible amounts of Pb remain soluble in pore solutions, as the leaching tests ascertained that the Pb leachability at pH 3.3 is a thou-

sand times higher than the specified limit.

In Fig. 6b, the Pb retention of CA samples at alkaline conditions is primarily assigned to the adsorption and ion exchange with ettringite and hematite or precipitation as $Pb(OH)_2$. At neutral pH conditions (pH 7 to 8), Pb leachability is dominated by hematite and ferrihydrite adsorption. Then Pb partially redissolves and reprecipitates as cerussite and anglesite, and a portion of soluble Pb remains in the pore solution in the forms of Pb^{2+}, $PbNO_3^-$, and $PbSO_{4(aq)}$ when the pH shifts to acid conditions. From Fig. 6c and d, the sulfates variation of OP and CA samples demonstrate a similar trend in acidic conditions (pH from 3 to 7). In these conditions, sulfate mainly precipitates as jarosite, anglesite, and gypsum. Whereas gypsum is the principal sulfate-bearing phase at pH values ranging from 7 to 9. The ettringite fraction increases at basic conditions, which are suitable for the stability of hydration products.

In general, our developed method enables a better understanding of the PTEs immobilization roles of the main hydration products and inherent phases in solid waste, which is hardly revealed by the experimental techniques. In turn, understanding the extent of this role variation will allow a more accurate and reliable mixture design for the in-situ remediation industry. The implications of these results underscore the importance of not only predicting and clarifying the PTEs immobilization amounts as a function of pH values but also highlighting the essential question of how the stabilized products would
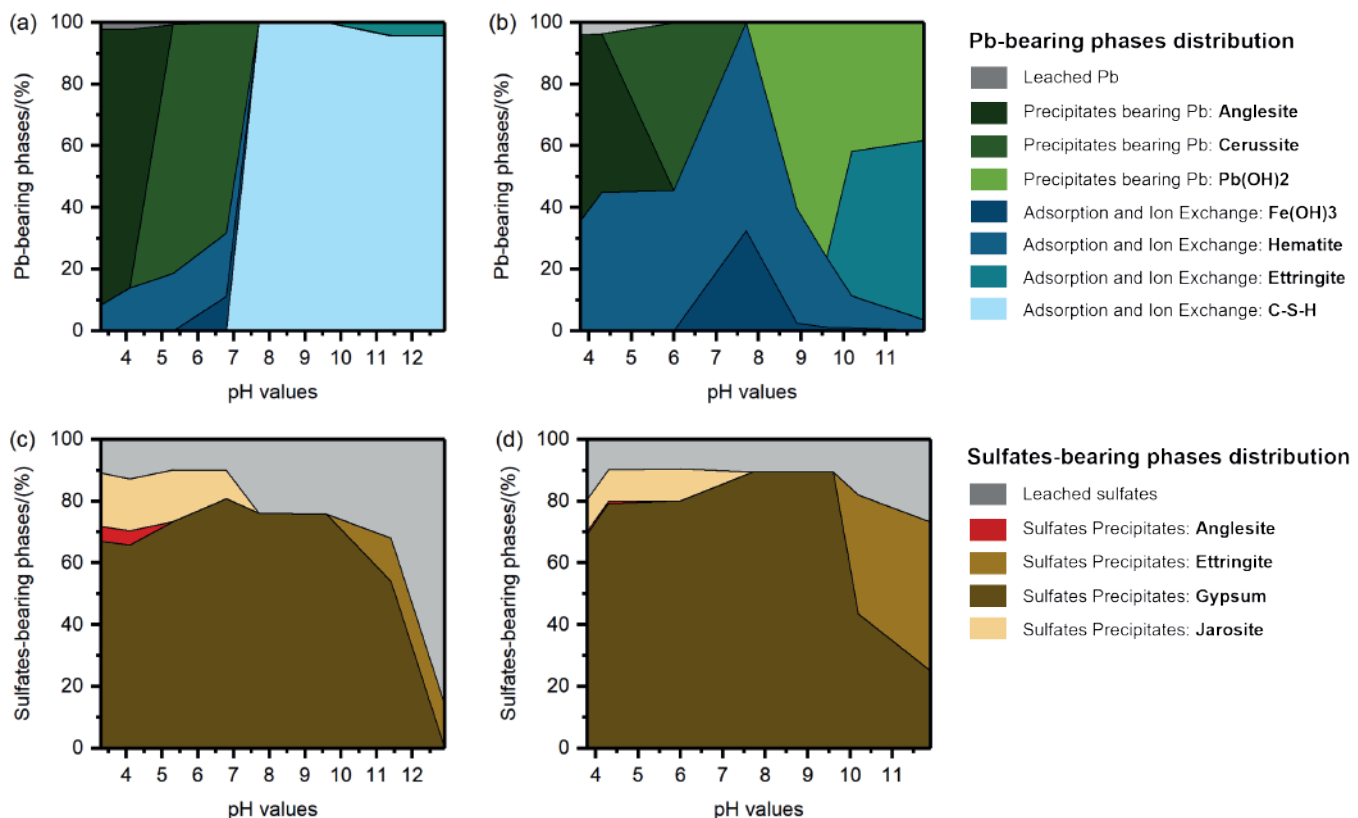

Figure 6 The simulated PTEs-bearing phases variation as a function of pH values. ***a)*** *The variation of the Pb-bearing species in OP.* ***b)*** *The variation of the Pb-bearing species in CA.* ***c)*** *The variation of the sulfates-bearing species in OP.* ***d)*** *The variation of the sulfates-bearing species in CA samples.*

contribute to PTEs retention when the field conditions are under harsh or unsuitable conditions. For example, when the pH of the rainfall and groundwater changes with the season or anthropogenic activities, the predicted concentrations of dissolved PTEs could be used to forecast whether secondary pollution will occur.

CONCLUSIONS

In this work, in-situ S/S has been proven a promising technology that can treat the PTEs contaminated soil profitably and scalably. Using the low-carbon binders to partially or entirely replace the use of ordinary Portland cement (OPC) has been proven a high-hope strategy that promotes the PTEs' remediation efficiency and bridges the gap between carbon-neutral world rhetoric and the reality of solid waste remediation applications. The developed geochemical modeling has prompted the possibility of an in-depth investigation for in-situ remediation in industrial sites by evaluating the PTEs leachability and the sponge effect of S/S products. The overall findings shed light on the understanding of PTEs immobilization mechanisms in multiple alternative sustainable binders, highlighting the significance of the perspectives of carbon neutrality in the emission-intensive S/S applications and providing new insights into the highly efficient S/S of contaminated wastes. The main conclusions are as follows:

(1) The characterization results demonstrate that Pb and Zn are the most abundant heavy metal pollutants within the collected pyrite ash samples. With the XRD, SEM/EDS, and Raman investigation, anglesite and kintoreite have been confirmed as the primary Pb-bearing crystalline phases, which may be generated from the oxidation of remaining pyrite particles. In addition, the jarosite could be a heavy metal hoster, as the Pb or Zn-incorporated jarosite was characterized along the edge of the hematite particles. The pH-dependent leaching tests and geochemical modeling reveal that the Pb and Zn leachability strongly depends on the pH values of the leachates, with a downward trend towards the near-neutral pH region from 6 to 10. At acid conditions, the increased solubility of Pb is dominated by the dissolution of anglesite and the formation of Pb nitrate complexes, while Zn is controlled by Zn ions and Zn-sulfate complexes in the solution. In contrast, when the pH values move to strong alkaline conditions, the upward trend could be associated with the complexation of aqueous metal hydrates. Noteworthy, the results indicate that even under normal conditions (for instance, normal rainfall), the stockpile of pyrite ash poses a great environmental risk and strongly threatens human health, which only worsens under acidic or alkaline conditions. Herein, integrating profitable and sustainable remediation technologies in the contaminated site is critically essential to prevent further pollution.

(2) In the S/S applications, the use of OPC is insufficient for efficient Pb immobilization due to the high alkaline conditions of the soil-binder system resulting from the dissolution of clinker phases, which may interfere with Pb precipitation. Meanwhile, the substantial carbon footprint attributed to OPC production also places critical scrutiny on this scenario. Although the CAC binder incorporation provides a promising Pb immobilization efficiency, the less satisfactory ecological benefits and the relatively high carbon footprint diminish the trial application of CAC. The GGBFS-incorporated binder tends to be a comprehensively sustainable and profitable strategy due to its excellent compatibility with Pb and relatively low-carbon nature. The experimental results indicate that aside from the Pb incorporation in the binding matrix similar to the OPC-waste system, the formation of low Ca/Si ratio C-(A)-S-H gel promoted the Pb retention, fulfilling the Pb leachability requirements for reuse as S/S material. Furthermore, the quantified sponge effect of industrial by-products incorporated pellets (MB and/or CB) suggests that it would promote the achievement of carbon neutrality. Overall, it provided useful guidance for improving the design and application of cement-free pathways for sustainable solid waste amendment, which bridged the gap between carbon-neutral world rhetoric and the reality of solid waste remediation applications.

(3) The pH-dependent leaching tests of CP and CA samples indicate both scenarios demonstrate high retention of Pb at neutral and alkaline pH conditions (approximately from 7 to 11). The use of CAC binder effectively enhanced the Pb retention capacity of the stabilized product, especially in harsh acid conditions, with only a quarter of Pb concentration detected in CA samples (11000 µg/L) compared to CP samples (43000 µg/L). Experiments reveal that Pb incorporation in OPP samples is mainly associated with the presence of C-S-H, with an observed enrichment in Ca and Si-rich areas along the cement particles (where C-S-H precipitation occurs), whereas the Pb is homogeneously distributed in the CA samples. Geochemical modeling reveals that C-S-H adsorption is the primary Pb immobilization mechanism of CP samples under alkaline conditions, with a 0.1 mol/mol Pb retention capacity that can be reached. When the pH is unsuitable for C-S-H precipitation, cerussite and anglesite precipitation are the main controls of Pb leachability, with small amounts of soluble Pb being adsorbed by hematite and ferrihydrite. Regarding the CA samples, precipitation of Pb(OH) and incorporation in ettringite are the primary control mechanisms for Pb equilibrium in alkaline environments. The Pb host capacity of ettringite is estimated

to be approximately 0.1 mol/mol, which is equivalent to C-S-H. However, the contribution of hematite and ferrihydrite adsorption to Pb equilibrium is observed in a broader pH range compared to OPP samples. Likewise, the cerussite and anglesite precipitation shows stronger affinities for Pb immobilization in acid conditions.

(4) The following works on revealing the physical profile would allow a more consistent description of the solid waste-binder systems. In addition, we recognize that the reliability and accuracy of our present model can be improved by further efforts of data collection in PTEs pH-dependent leachability with different PTEs concentrations and different mixtures proportions. Should the changes be significant, the model will need to be re-assessed and re-calibrated.

REFERENCES

Berthomier, M., Lors, C., Damidot, D., De Larrard, T., Guérandel, C., & Bertron, A. (2021): Leaching of CEM III paste by demineralised or mineralised water at pH 7 in relation with aluminium release in drinking water network. *Cem. Concr. Res*, **143**, 106399.

Bizzozero, J., Gosselin, C., & Scrivener, K.L. (2014): Expansion mechanisms in calcium aluminate and sulfoaluminate systems with calcium sulfate. *Cem. Concr. Res*, **56**, 190–202.

Bonomo, L., Careghini, A., Dastoli, S., De Propris, L., Ferrari, G., Gabellini, M., & Saponaro, S. (2009): Feasibility studies for the treatment and reuse of contaminated marine sediments. *Environ. Technol*, **30**, 817–823.

Calgaro, L., Contessi, S., Bonetto, A., Badetti, E., Ferrari, G., Artioli, G., & Marcomini, A. (2021): Calcium aluminate cement as an alternative to ordinary Portland cement for the remediation of heavy metals contaminated soil: mechanisms and performance. *J. Soils Sediments*. **21**, 1755–1768

Chen, Q.Y., Tyrer, M., Hills, C.D., Yang, X.M., & Carey, P., (2009): Immobilisation of heavy metal in cement-based solidification/stabilisation: A review. *Waste Manag.*, **29**, 390-403.

Contessi, S., Calgaro, L., Dalconi, M.C., Bonetto, A., Bellotto, M. Pietro, Ferrari, G., Marcomini, A., & Artioli, G. (2020): Stabilization of lead contaminated soil with traditional and alternative binders. *J. Hazard. Mater*, **382**, 120990.

Du, B., Li, J., Fang, W., & Liu, J., (2019): Comparison of long-term stability under natural ageing between cement solidified and chelator-stabilised MSWI fly ash. *Environ. Pollut.*, **250**, 68–78.

Gardner, L.J., Bernal, S.A., Walling, S.A., Corkhill, C.L., Provis, J.L., & Hyatt, N.C. (2015): Characterisation of magnesium potassium phosphate cements blended with fly ash and ground granulated blast furnace slag. *Cem. Concr. Res*, **74**, 78–87.

Habert, G., Miller, S.A., John, V.M., Provis, J.L., Favier, A., Horvath, A., & Scrivener, K.L. (2020): Environmental impacts and decarbonization strategies in the cement and concrete industries. *Nat. Rev. Earth Environ*, **111**, 559–573.

Hidalgo, A., García Calvo, J.L., Alonso, M.C., Fernández, L., & Andrade, C. (2009): Microstructure development in mixes of calcium aluminate cement with silica fume or fly ash. *J. Therm. Anal. Calorim*, **96**, 335–345.

Hou, D., Al-Tabbaa, A., O'Connor, D., Hu, Q., Zhu, Y.G., Wang, L., Kirkwood, N., Ok, Y.S., Tsang, D.C.W., Bolan, N.S., & Rinklebe, J. (2023): Sustainable remediation and redevelopment of brownfield sites. *Nat. Rev. Earth Environ*, **44**, 271–286.

Kirca, Ö., Özgür Yaman, I., & Tokyay, M. (2013): Compressive strength development of calcium aluminate cement–GGBFS blends. *Cem. Concr. Compos*, **35**, 163–170.

Li, G., Zhang, A., Song, Z., Shi, C., Wang, Y., & Zhang, J. (2017): Study on the resistance to seawater corrosion of the cementitious systems containing ordinary Portland cement or/and calcium aluminate cement. *Constr. Build. Mater*, **157**, 852–859.

Liu, Y., Molinari, S., Dalconi, M.C., Valentini, L., Ricci, G., Carrer, C., Ferrari, G., & Artioli, G. (2023): The leaching behaviors of lead, zinc, and sulfate in pyrite ash contaminated soil: mineralogical assessments and environmental implications. *J. Environ. Chem. Eng*, **11**, 109687.

Liu, Y., Molinari, S., Dalconi, M.C., Valentini, L., Bellotto, M.P., Ferrari, G., Pellay, R., Rilievo, G., Vianello, F., Salviulo, G., Chen, Q., & Artioli, G. (2023): Mechanistic insights into Pb and sulfates retention in ordinary Portland cement and aluminous cement: accessing the contributions from binders and solid waste. *J. Hazard. Mater.*, **458**, 131849.

Ouhadi, V.R., Yong, R.N., & Deiranlou, M. (2021): Enhancement of cement-based solidification/stabilization of a lead-contaminated smectite clay. *J. Hazard. Mater.*, **403**, 123969.